

Through-focus Scanning and Scatterfield Optical Methods for Advanced Overlay Target Analysis

Ravikiran Attota, Michael Stocker, Richard Silver, Alan Heckert,
Hui Zhou[#], Richard Kasica, Lei Chen, Ronald Dixson,
George Orji, Bryan Barnes and Peter Lipscomb*

National Institute of Standards and Technology
Gaithersburg, MD 20899-8212, USA

[#]KT Consulting Inc, Antioch, CA, USA

*International Sematech, Austin, TX 78741

ABSTRACT

In this paper we present overlay measurement techniques that use small overlay targets for advanced semiconductor applications. We employ two different optical methods to measure overlay using modified conventional optical microscope platforms. They are scatterfield and through-focus scanning optical microscope (TSOM) imaging methods. In the TSOM method a target is scanned through the focus of an optical microscope, simultaneously acquiring optical images at different focal positions. The TSOM images are constructed using the through-focus optical images. Overlay analysis is then performed using the TSOM images. In the scatterfield method, a small aperture is scanned at the conjugate back focal plane of an optical microscope. This enables angle-resolved scatterometry on a high-magnification optical platform. We also present evaluation of optical constants using the scatterfield method.

Keywords: Overlay, Scatterfield, Scatterometry, TSOM, In-chip, Through-focus, Optical constants

1. INTRODUCTION

As critical dimensions continue to decrease, it becomes increasingly desirable to have overlay targets that emulate the spatial frequency of the actual devices to improve overlay measurement accuracy. Traditional overlay targets are relatively large and cannot be placed in the active area of a chip due to process constraints. Therefore, it is also desirable to have relatively small overlay targets that are more suitable to placement in the active area of chip.

In this paper we present overlay measurements using two types of overlay targets. They are (i) dense overlay targets composed of device-sized features and (ii) what is commonly referred to as in-chip overlay targets. Although both target flavors can be designed with features that emulate actual device spatial characteristics, the in-chip targets specifically are intended to minimize overall target size. We employ two different optical methods to measure overlay using modified conventional optical microscope platforms. They are scatterfield [1-3] and through-focus scanning optical microscope (TSOM) imaging [4-6] methods. In the scatterfield method, a small aperture is scanned at the conjugate back focal plane of an optical microscope. This enables angle-resolved scatterometry on a high-magnification optical platform. In the TSOM method a target is scanned through the focus of an optical microscope, simultaneously acquiring optical images at different focal positions. The TSOM images are constructed using the through-focus optical images. Overlay analysis is then performed using the TSOM images.

Overlay measurement based on scatterometry methods has shown promise [7]. However, traditional scatterometry based methods require relatively large targets. Because magnification optics are used with the scatterfield microscopy approach, significantly smaller scatterometry targets can be measured. This also enables one to simultaneously measure

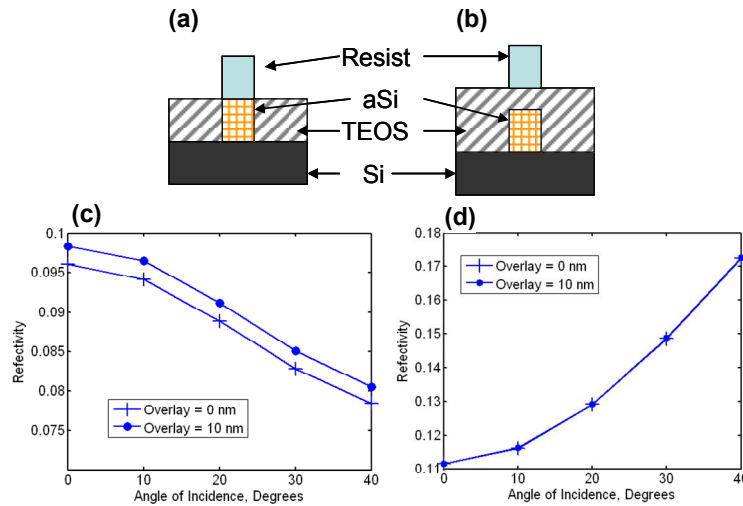


Figure. 1 The dense scatterometry type overlay target design: (a) with out, and (b) with intermediate layer between the two levels. Simulated angle resolved reflectivity for (c) no intermediate layer, and (d) 100 nm intermediate layer. Pitch = 200 nm, Line width = 50 nm, Line height = 100 nm, Wavelength = 546 nm, Si lines on Si substrate. Electric field perpendicular to the lines.

several smaller scatterometry overlay targets that fit in the field of view of the microscope. We will present an experimental and simulation based study of overlay measurements using scatterfield techniques.

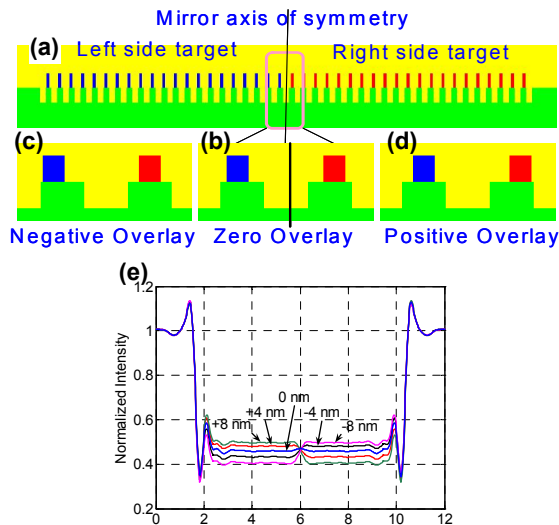


Figure. 2 (a) The overlay target design with gratings of the same pitch at two levels with an axis of mirror symmetry. (b), (c), and (d) Enlarged view of the center of the target (a) for zero, negative and positive overlay, respectively. (e) Simulated optical intensity profiles for the different overlay values. Pitch = 200 nm, Line width = 50 nm, Line height = 100 nm, Trench width = 100 nm, Trench depth = 100 nm, Illumination numerical aperture = 0.4, Collection numerical aperture = 0.8, Wavelength = 546 nm, Unpolarized illumination, Si lines on Si substrate.

In an alternative approach, we used the TSOM imaging method to analyze overlay using small in-chip overlay targets. Analysis of the TSOM images provides quantitative evaluation of the physical overlay. Experimental examples with different offsets will be presented in the paper.

Before going into overlay measurements using small target geometries, in the following section we discuss the effect of interfacial layers on the overlay measurement sensitivity when measuring targets that produce zeroth order imaging. Interfacial layers have a significant effect on overlay measurement accuracy and sensitivity when measuring dense arrayed overlay targets.

2. ZEROTH ORDER TARGETS FOR OVERLAY MEASUREMENT

Under specific measurement conditions, it is essential that features on the two levels for which overlay is being measured must be optically interacting. This optical interaction is especially important for a target design with zeroth order imaging. Here we present the effects from two types of optical interactions on overlay sensitivity. They are (i) horizontal, and (ii) vertical optical interactions.

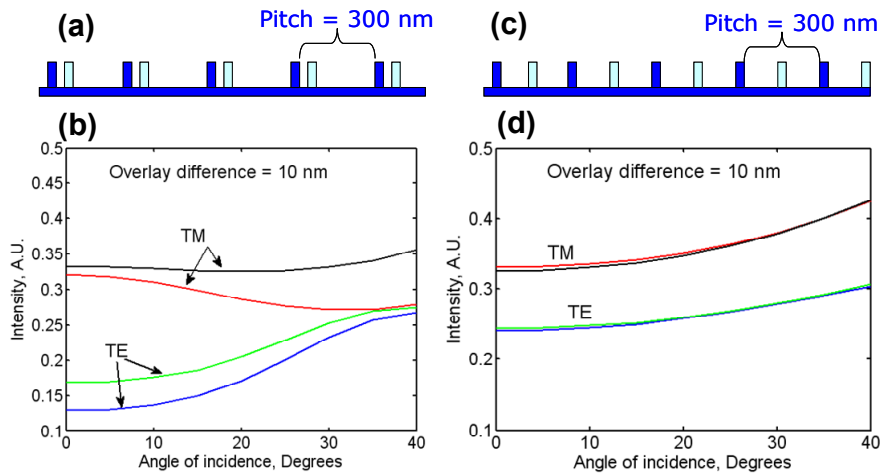


Figure 3 (a) Overlay target design with optical proximity. (b) Simulated angle resolved intensity curves for 10 nm difference in the overlay for the target in (a). (c) Overlay target design with minimal optical proximity. (d) Simulated angle resolved intensity curves for 10 nm difference in the overlay for the target in (c). Line width = 40 nm, Line height = 100 nm, Wavelength = 193 nm, Si lines on Si substrate.

2.1 Vertical Interaction

Overlay targets contain features that are generally from two process levels. For a grating type of overlay target these features can be overlay features from one level directly on top of features from another level as shown in Fig. 1(a). In this design the resist lines are centered over the amorphous Si (aSi) lines for zero nm overlay. For a given overlay, the resist lines move horizontally with respect to the aSi lines. In a second case the two levels are separated with an intermediate layer as shown in Fig. 1(b). Using these two target designs we present the importance of vertical optical interaction for overlay sensitivity, particularly for dense structures, i.e. grating type targets that produce only zeroth order specular reflection under a given experimental condition. Angle resolved reflectivity for the grating type of overlay target shown in Fig. 1(a) is shown in Fig. 1(c) for zero nm and 10 nm overlay. The figure shows a clear distinction in reflectivity curves between the two overlay values. However, when an intermediate layer separates the two levels as shown in Fig. 1(b), the angle resolved reflectivity shows negligible sensitivity to overlay as shown in Fig. 1(d).

One explanation for the lack of sensitivity to overlay for targets with the intermediate layer is that the level of optical interaction between the two features in the two process levels is not adequate. When the features are one over the other as in Fig. 1(a), sufficient optical interaction produces the sensitivity to overlay. The results in this figure demonstrate the important effect that a dense upper level grating can prevent propagation of the lateral position information from reaching the lower level. This has the profound effect of not allowing the lateral position information contained in the higher order optical content from both propagating from the upper level to the lower level and in turn reflecting back through the upper level. Using a thinner intermediate layer to ensure optical coupling can then enable the propagation of the lateral position information.

We show a second example of an overlay target design that demonstrates the importance of vertical optical interaction. In Figure 2 we present an overlay target design that produces zeroth order imaging. The lower level consists of trenches of parallel lines in a Si substrate with a pitch of 200 nm. The upper level consists of Si lines with the same pitch of 200 nm, except that there is a discontinuity of pitch at the center of the target such that the left side of the target is a mirror image of the right side of the target as shown in Fig. 2(a). A magnified image of the center of the target is shown in Fig. 2(b), for zero overlay. For a given finite overlay of the top level with respect to the lower level, the mirror symmetry at the center of the target is lost as shown in Figs. 2(c) and (d) for negative and positive overlays, respectively. For an illumination wavelength of 546 nm, this target produces zeroth order reflectivity from the central region of the dense lines.

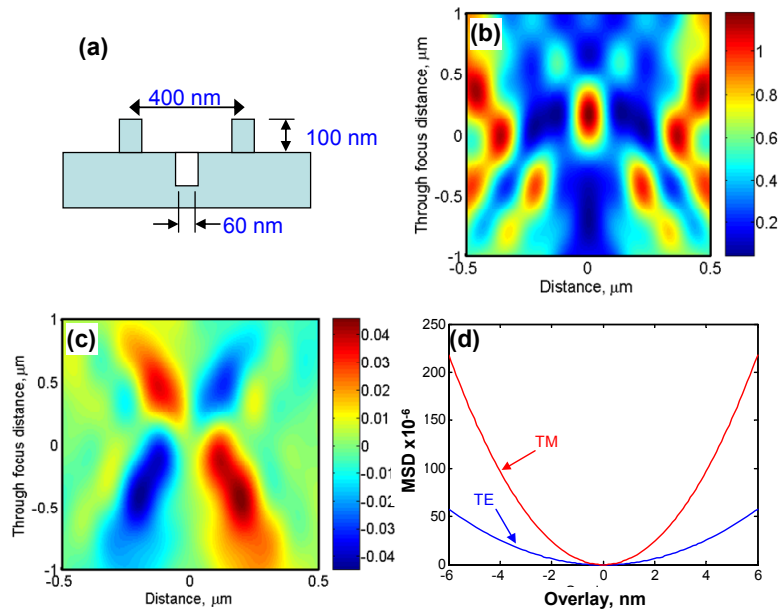


Figure 4. (a) In-chip overlay target. (b) Simulated TSOM image for the in-chip target with 6 nm overlay. (c) Simulated differential TSOM image for 6 nm overlay. (d) Calibration overlay curves generated using simulations for the in-chip target shown in (a). Illumination numerical aperture = 0.2, Collection numerical aperture = 0.8, Wavelength = 193 nm, Si lines on Si substrate.

Intensity profiles acquired from the optical images for different overlay values are shown in Fig. 2(e). The axis of symmetry for the overlay target corresponds to a distance of 6 μm in Fig. 2(e). From this figure we can observe that for a zero overlay the left side optical intensity is equal to the right side optical intensity. For a positive overlay value, the left side optical intensity increases, while the right side optical intensity decreases. A reverse effect can be observed for the negative overlay values. The difference in the left and the right side optical intensities increases with increasing the overlay value.

The overlay target design shown here does not have an intermediate layer between the lower and the upper levels. This design allows optical interaction between the upper and the lower levels, i.e. vertical interaction, and exhibits sensitivity to overlay. However, if an intermediate layer is inserted between the upper and the lower level, the sensitivity to overlay disappears due to the lack of propagation of the lateral position information. Irrespective of the overlay value, the left and the right side of the optical intensities remain the same, highlighting the detrimental effect of the intermediate layer on vertical optical interactions and hence overlay measurements.

2.2 Horizontal Interaction

In this section we present an example that demonstrates the importance of the horizontal optical interactions for overlay measurements. In Fig. 3(a) we present an overlay target design where alternate lines are printed in two different steps (as in double patterning) constituting an overlay. If the design is such that the lines in two steps are optically close and interacting as shown in Fig. 3(a), then a 10 nm overlay shows good sensitivity as measured by scatterometry/scatterfield type of instrument as shown in Fig. 3(b). However, if the two sets of lines are optically far away as shown in Fig. 3(c), limited optical interaction can be expected. This produces a small sensitivity to overlay as shown in Fig. 3(d) for 10 nm overlay. Therefore, it is critical for dense features to have appropriate optical interaction, both horizontally and vertically, to show sensitivity to overlay.

In the following sections we present the two optical methods for measurement of small overlay targets.

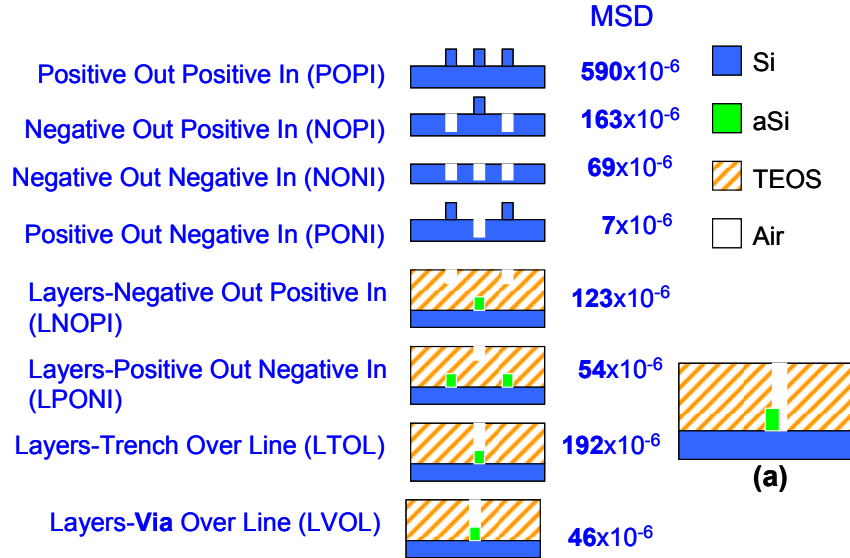


Figure 5. Cross sections of different configurations of in-chip type of targets with zero overlay and the corresponding MSD values for a 10 nm overlay (a) Depiction of finite overlay for LTOL or LVOL type of targets. Pitch = 200 nm, Line width = 50 nm, Line height = 100 nm, Trench width = 100 nm, Trench depth = 100 nm; TEOS thickness = 300 nm, Illumination numerical aperture = 0.27, Collection numerical aperture = 0.8, Wavelength = 193 nm, Electric field perpendicular to the lines.

3. OVERLAY ANALYSIS FOR IN-CHIP TYPE OF TARGETS USING THROUGH-FOCUS SCANNING OPTICAL MICROSCOPE IMAGING METHOD

Previously we published the initial demonstration of the TSOM imaging method using a different name, the “through focus image map” method [4]. Subsequently, we presented a detailed description of the method with various applications, including experimental validation [5,6]. For the sake of clarity we present a brief description of the method here. The TSOM imaging method consists of initially acquiring a set of optical images at different defocus positions by scanning a target along the focus direction using an optical microscope. The optical intensity profiles of the acquired images are then stacked at their respective defocus positions to form a TSOM image. The TSOM image is sensitive to changes in the dimensions of the target being imaged, including overlay. As a result we next describe a method to analyze overlay using the TSOM images for in-chip type of overlay targets.

One of the geometries of a typical in-chip overlay target is shown in Fig. 4(a). It consists of three line features. For the case presented in Fig. 4(a) the outer two lines are in the upper process level while the inner trench is in the lower process level constituting an overlay target. For a given overlay, the inner trench moves horizontally with respect to the outer two lines. Previously, overlay measurements of the in-chip type overlay targets were completed using the best-focus image [8].

The simulated TSOM image for the target shown in Fig.4(a) is shown in Fig. 4(b) for 6 nm overlay. The TSOM image for a different overlay value appears similar to the one shown in Fig. 4(b). However, the difference in the overlay can be highlighted by evaluating the differential TSOM images for any two different overlay values. Such a differential image for a 6 nm difference in the overlay is shown in Fig. 4(c), which visually represents or highlights the differences in the optical intensities at different defocus positions. In order to quantify the overlay difference we evaluate the mean square difference (MSD) from the differential image using the following equation.

$$MSD = \frac{\sum_{i=1}^n (TSOM1_i - TSOM2_i)^2}{n}$$

where TSOM1 and TSOM2 are the TSOM images for nominally zero and a given overlay value, respectively, and n is the total number of pixels in the TSOM image. The value of the MSD increases with increasing overlay value. A plot of the MSD as a function of the overlay value results in a calibration curve as shown in Fig. 4(d). The calibration curve generated by such a method is specific to the in-chip target geometry under the given experimental conditions. Such a calibration curve can be generated either using simulations or experimentally, by measuring targets with known overlay. To evaluate the overlay value of an in-chip type of target with an unknown overlay offset we compared its MSD value with that of the calibration curve. Under the given experimental conditions here, TM polarization produces higher sensitivity to overlay compared to TE polarization as shown in Fig. 4(d).

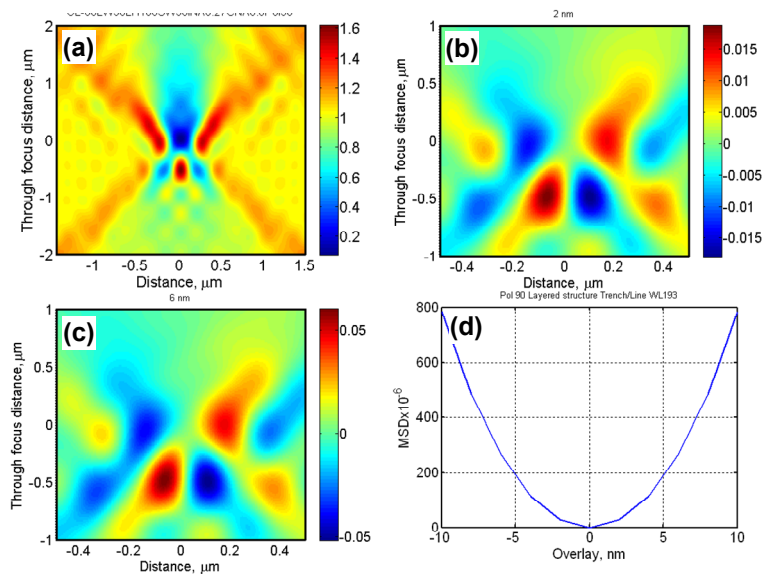


Figure 6. (a) Simulated TSOM image for LTOL type of in-chip target. The differential TSOM image for (b) 2 nm, and (c) 6 nm overlay. (d) The simulated overlay calibration curve. aSi Line width = 100 nm, aSi Line height = 100 nm, Trench width in TEOS = 100 nm, Trench depth in TEOS = 200 nm; TEOS thickness = 300 nm, Illumination numerical aperture = 0.27, Collection numerical aperture = 0.8, Wavelength = 193 nm, Electric field perpendicular to the lines.

Several geometrical configurations of in-chip type of targets are possible as shown in Fig. 5, each one producing a different sensitivity to overlay under the given experimental conditions. From Fig. 5 we can observe that the positive-out-positive-in type of overlay target produce the highest sensitivity to overlay, while positive-out-negative-in type of overlay targets produce the lowest sensitivity. These in-chip type of targets produce sensitivity to overlay even when an intermediate layer is present as shown in Fig. 5 for layers-negative-out-positive-in and layers-positive-out-negative-in type of targets, since these targets intrinsically generate high order optical content.

We also evaluated a single line per level in-chip type of target as shown in Fig. 5, layers-trench-over-line (LTOL) and layers-via-over-line (LVOL) targets. This type of target is most suitable for contacts/via overlay metrology. For the target geometry shown in Fig. 5, they consist of trenches or vias etched in a layer of TEOS to make contact with the buried line of amorphous Silicon (aSi). For zero overlay, the center of trench or via structures matches with the center of the aSi line. For a given overlay, the trench or via features move horizontally with respect to the aSi line as shown in Fig. 5(a). A change in the overlay value produces a change in the TSOM image that enables measurement of the overlay value.

In Fig. 6 we present simulation results for overlay measurement using a single line LTOL target. A typical TSOM image is shown in Fig. 6(a) for zero overlay offset. Here we present targets having 3 μm total dimension on the x-axis and 4 μm total focus range on the y-axis (3 μm x 4 μm of TSOM image). However, the differential image produces most of the content in the 1 μm x 2 μm central area of the TSOM image as shown in Fig. 6(b) for 2 nm overlay. The differential image for 6 nm overlay appears similar to 2 nm overlay as shown in Fig. 6(c), except that the z-scale increases as seen

from the color-bar-scale on the right side of the images. This increase in the z-scale with overlay produces higher MSD value even though the differential images have a similar appearance. A typical calibration curve thus obtained for LTOL target is shown in Fig. 6(d), for use in the measurement of unknown overlay of a LTOL target under the given conditions.

S.No.	Line Width (nm)	Line Height (nm)	Overlay Difference (nm)	MSD $\times 10^{-6}$	Percentage Difference in MSD	Error in Overlay (nm)
1	100	100	4	21.7		
2	100	105	4	22.3	1.5	0.06
3	104	100	4	21.3	0.8	0.032
4	104	105	4	22.5	1.95	0.078

Table 1. Table showing error in the overlay measurement due to process variations for NOPI type of in-chip target. Line width = 100 nm, Line height = 100 nm, Trench width = 100 nm, Trench depth = 100 nm; Illumination numerical aperture = 0.27, Collection numerical aperture = 0.8, Wavelength = 546 nm, Electric field perpendicular to the lines.

3.1 Robust to Process Variation

It is important to evaluate how robust are overlay measurements using the TSOM imaging method. In practice it is common to have process variations that produce small changes in the dimensions of the metrology targets, including the overlay measurement targets. In Table 1 we present simulation results to test robustness in overlay measurement using the TSOM imaging method for the negative-out-positive-in type of in-chip target. For this target, an initial calibration curve was generated using the desired line width and line height of 100 nm. For a 4 nm overlay this target produces an MSD value of 21.7×10^{-6} as shown in Table 1 for this set of experimental conditions. A 5 nm change in the line height due to process variations produces the MSD value of 22.3×10^{-6} , which results in 0.06 nm of error in the overlay measurement. Similarly a 4 nm difference in the line width produces an overlay error of 0.032 nm. This example shows a relatively small error in the overlay measurement due to process variations and hence makes this method robust for the example conditions studied here.

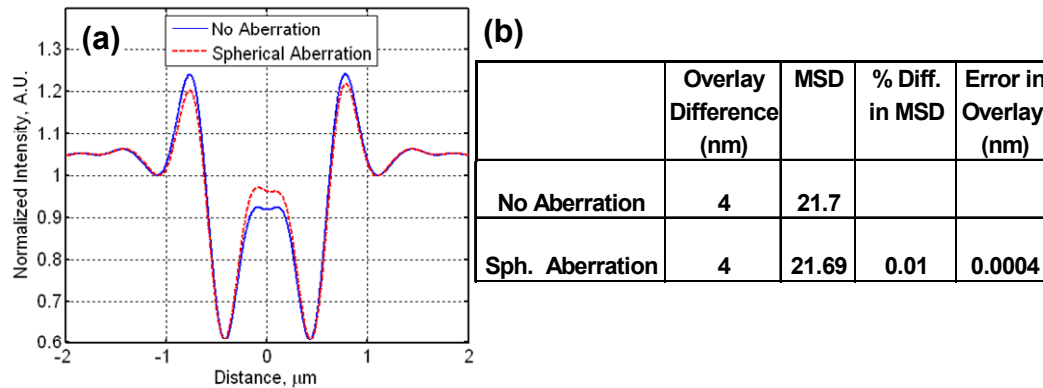


Figure 7. (a) Intensity profiles of NOPI type of in-chip targets with and without spherical aberrations. (b) Table showing error in the overlay measurement due to the presence of spherical aberration. Line width = 100 nm, Line height = 100 nm, Trench width = 100 nm, Trench depth = 100 nm; Illumination numerical aperture = 0.27, Collection numerical aperture = 0.8, Wavelength = 546 nm, Electric field perpendicular to the lines.

3.2 Robust to Optical Aberrations

All optical tools have optical aberrations, some to a lesser degree and some to a greater degree. Although it may be possible to evaluate many of the optical aberrations in a given optical system and account for these aberrations in the simulations of the calibration curves, in many cases it may not be possible to evaluate all of the possible optical aberrations. In either case, it is important to know the degree to which error is introduced in the measurement of overlay due to presence of optical aberrations.

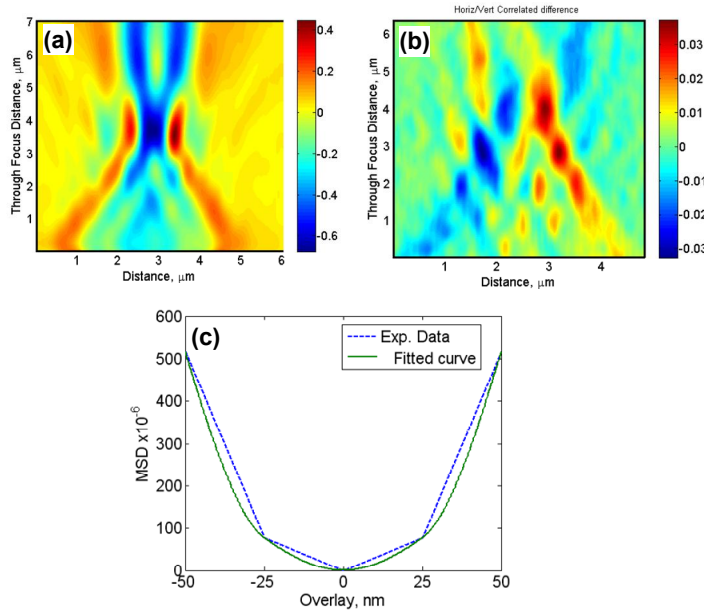


Figure 8. Experimental (a) TSOM image, (b) differential TSOM image for 20 nm overlay, and (c) calibration curve for NOPI type of in-chip target. Pitch = 2.12 μm , Line width = 89.5 nm, Line height = 102 nm, Trench width = 90 nm, Trench depth = 135 nm; Illumination numerical aperture = 0.27, Collection numerical aperture = 0.8, Wavelength = 546 nm, Electric field perpendicular to the lines.

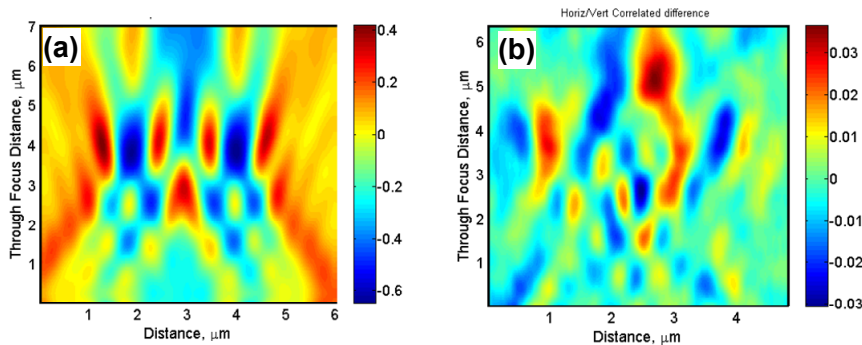


Figure 9. Experimental (a) TSOM image, (b) differential TSOM image for 20 nm overlay for LNOPI type of in-chip target. Pitch = 2.12 μm , Line width = 89.5 nm, Line height = 102 nm, Trench width = 90 nm, Trench depth = 135 nm; TEOS thickness = 270 nm, Illumination numerical aperture = 0.27, Collection numerical aperture = 0.8, Wavelength = 546 nm, Electric field perpendicular to the lines.

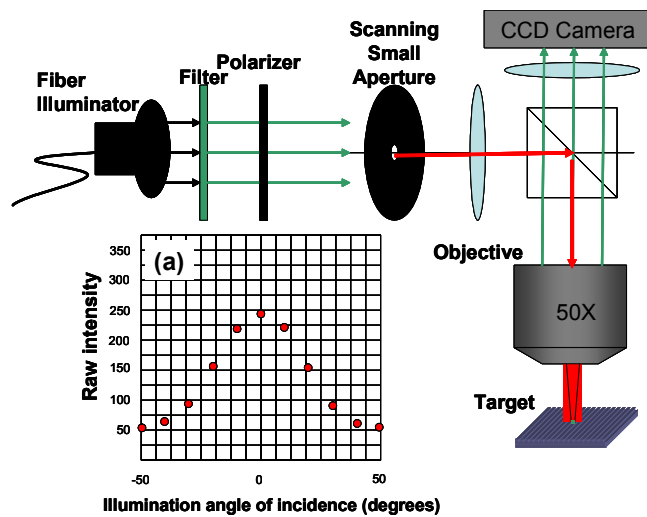


Figure 10. Schematic representation of the scatterfield microscope. (b) A typical angle-resolved reflection curve obtained using the scatterfield microscope.

To study this, we first evaluated a calibration curve under the conditions for the target shown in Table 1 for an aberration-free optical system. The optical intensity profile at the best focus position for such a system is shown in Fig. 7(a) for zero overlay. The intention is to use the calibration curve so obtained to measure overlay using an optical system that has aberration, for example spherical aberration. We then evaluated TSOM images using a third order spherical aberration with Zernike coefficient of 0.01. The optical intensity simulated with the programmed spherical aberration at the best focus position is plotted in Fig. 7(a) along with the aberration-free profile. We can observe considerable difference between the two intensity profiles. However, the evaluated MSD under the two conditions shows a very small variation for a 4 nm overlay as shown in Fig. 7(b). The error in the overlay measurement is negligible under the experimental conditions indicating this method is robust to optical aberration. In the following sections we present the experimental results.

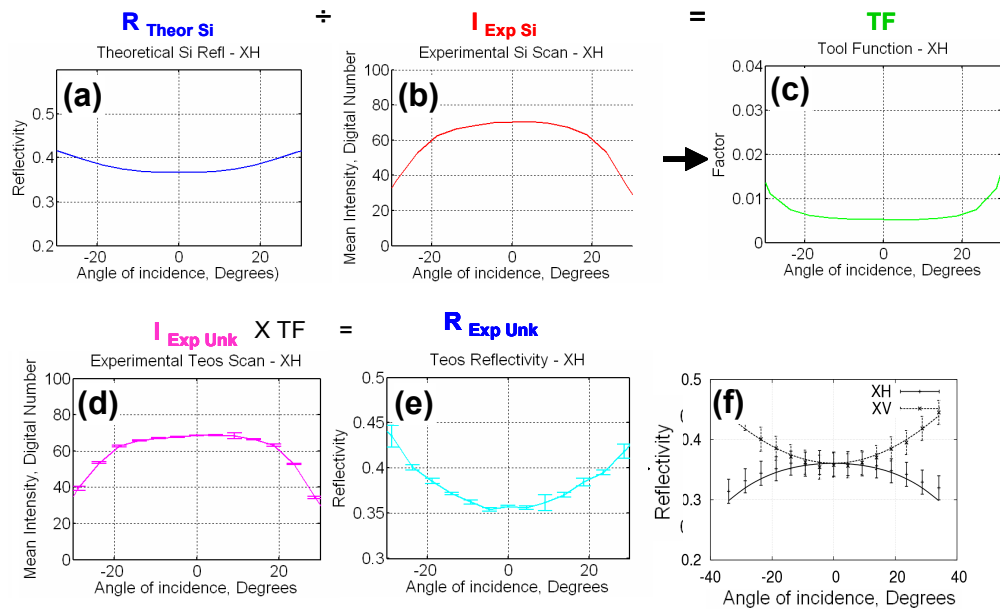


Figure 11. (a) Theoretical reflection curve for blank Si. (b) Experimental scatterfield curve obtained for the blank Si. (c) Tool function obtained by dividing the theoretical reflection curve with the experimental reflection curve. (d) Experimental scatterfield curve obtained for a blank unknown material. (e) Theoretical reflection curve obtained by applying tool function on (d). (f) Evaluation of the optical constants of the unknown material by the best fit library matching method. Curves are from the simulations and points are from the experiments. The error bars represent experimental repeatability. Wavelength = 546 nm, XH = Electric field perpendicular to the lines, XV = Electric field parallel to the lines.

3.3 Experimental Validation

Following the procedure described above we evaluated a calibration curve for the negative-out-positive-in type of in-chip target shown in Fig. 5. The experimental TSOM image of the in-chip target is shown in Fig. 8(a). The differential image for zero and 20 nm overlay is shown in Fig. 8(b), which results in the MSD value of 73×10^{-6} under the given experimental conditions. The experimental calibration curve obtained using the different overlay targets is shown in Fig. 8(c). Using the experimental calibration curve aids in evaluating unknown overlay values for similar target types and experimental conditions assuming linearity is maintained in the response.

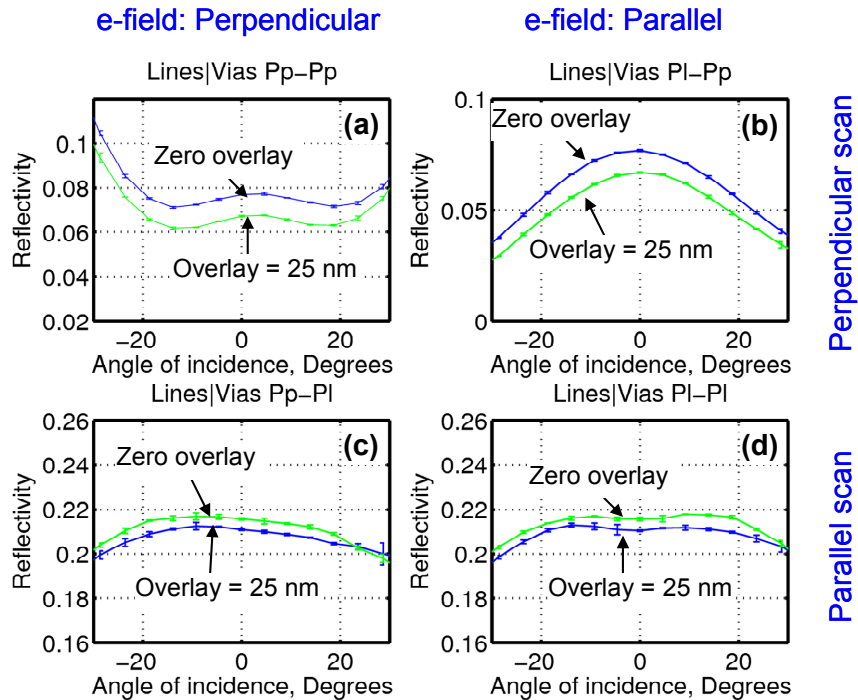


Figure 12. Experimental scatterfield curves obtained in the two scan directions for the two polarizations using vias over lines (LVOL) type of grating target. Wavelength = 546 nm.

A second type of layer, negative-out-positive-in overlay target from Fig.5 was also experimentally tested. The outer two lines are trenches in a TEOS upper layer and the inner line is an aSi line buried under the TEOS layer. The experimental TSOM image obtained is shown in Fig. 9(a) and the experimental differential image for 20 nm overlay is shown in Fig. 9(b). For a 20 nm overlay, this target results in the experimental MSD value of 83×10^{-6} .

4. OVERLAY ANALYSIS FOR SCATTEROMETRY TYPE OF TARGETS USING SCATTERFIELD MICROSCOPY METHOD

Scatterometry has become an increasingly useful tool for optical nanometrology, especially in the semiconductor industry. However, current hardware requires a relatively large target size for meaningful analysis. Following the discussion above, current and future overlay metrology measurements are pushing the need for smaller target size. Scatterfield microscopy [1-3] is suitable to make overlay measurements using small targets. Making scatterometry type (angle resolved) measurements using a high magnification, bright field optical microscope platform enables the scatterfield microscopy technique. A small scanning aperture is placed at the conjugate back focal plane of an optical microscope to produce a near-plane wave illumination at the sample plane at different angles of incidence as shown in Fig. 10. The position of the scanning aperture determines the angle of incidence. The main advantage of using the scatterfield microscopy platform is that the magnification allows measurement of very small overall target geometries. In fact recent results using a 193 nm tool scatterfield microscope show targets can be as small as $2 \mu\text{m} \times 2 \mu\text{m}$ and still be adequate for metrology purposes.

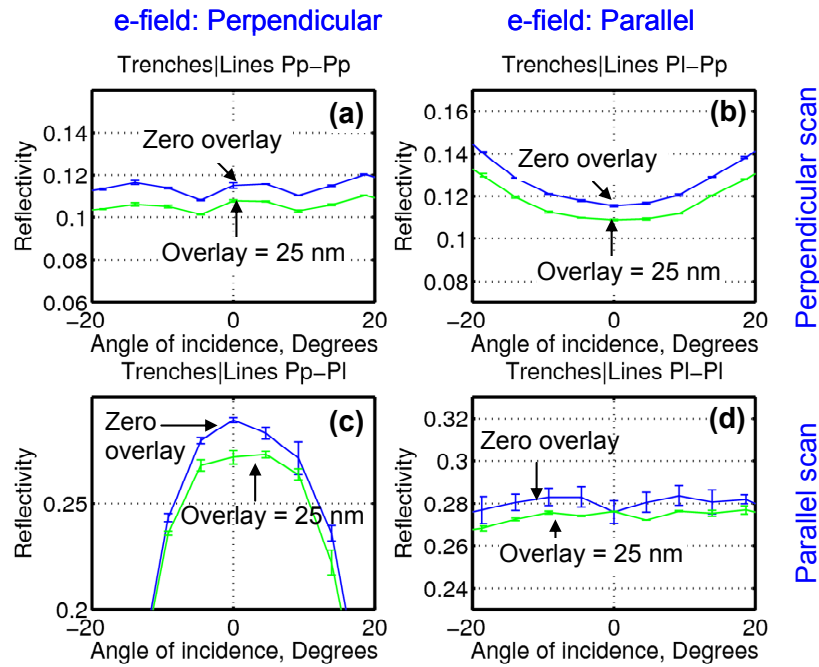


Figure 13. Experimental scatterfield curves obtained in the two scan directions for the two polarizations using trenches over lines (LTOL) type of grating target. Wavelength = 546 nm.

In the current section we perform analysis of scatterometry-type grating targets having only zeroth order imaging present. A typical angle resolved intensity measured at the CCD camera is shown in Fig. 10(a). This curve requires proper normalization to enable accurate comparison with simulations. The intensity of the light source, the numerous lenses used in the optical train and the angle dependent transmission of the light through the optics affect the experimental intensity profile obtained at the camera. We implement a 'tool function' to capture and normalize these effects relative to a known silicon reflectivity curve. This allows the experimental intensity profile to be compared with simulation on an absolute scale.

Successful application of this method involves two steps: (i) to obtain the tool function, and (ii) to apply the tool function to the experimental curve. As an example, to obtain the tool function for the optical microscope used in the current work we carried out the following procedure. We selected a blank Si substrate whose optical constants were well characterized. We obtained angle-resolved simulated reflectivity curves and experimental angle-resolved intensity curves for the Si target as shown in Fig. 11(a) and (b), respectively. Dividing the experimental profile by the simulated profile point-by-point results in the tool function for the optical microscope used, as shown in Fig. 11(c). The tool function is specific to a given tool under the given experimental conditions. Two scanning directions with two polarizations produce a total of four tool functions.

Once the tool functions are evaluated, they can be applied to the experimental curves of any target with unknown optical constants and geometry (derived here only for zeroth order imaging conditions) to obtain the experimental reflectivity curves. We applied the tool functions to the experimental curves obtained for a blank TEOS layer to obtain their experimental reflectivity curves as shown in Figs. 11 (d) and (e). A blank layer does not require scanning in the two directions. Therefore, for the blank TEOS layer we obtained two reflectivity curves for the two polarizations. Once the two reflectivity curves have been evaluated, they can be compared to a library of simulations to obtain the best-matched conditions. In this way, optical properties, thickness and other dimensions of the targets can be evaluated. Using the same procedure we evaluated the thickness and the optical constants for the TEOS layer as $n = 1.622$ and $k = 0$ and thickness = 88 nm as shown in Fig. 11(f). This evaluation of optical constants and layer thickness is essential to obtain robust accurate measurements of complication multi-level overlay targets,

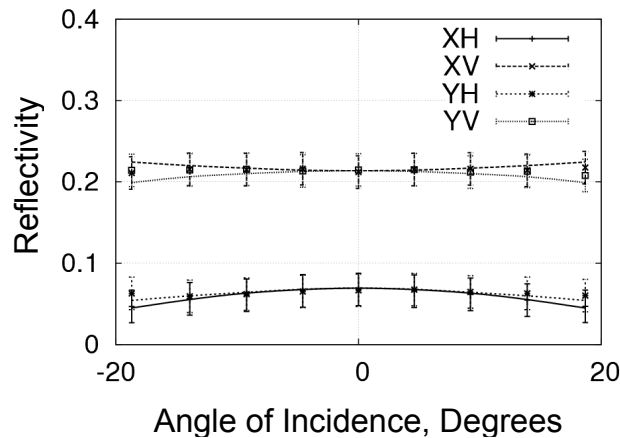


Figure 14. Six parameter best fit obtained for the overlay stack. XH = Perpendicular scan and perpendicular e-field, XV = Perpendicular scan and parallel e-field, YH = Parallel scan and perpendicular e-field, YV = Parallel scan and parallel e-field. The curves are from the simulations and the points are from the experiments.

4.2 Parametric fitting to the overlay stack

Having determined the experimental sensitivity to overlay using the scatterfield method, we then made an initial attempt to fit the experimental scatterfield curves of the first type of target stack with that of the simulations. This stack consists of a Si substrate, aSi lines and a TEOS covering layer. To make the parametric fit we need to identify the starting point parameter values and ranges for all of the unknown variables. The floating variables identified are the optical constants and layer thickness of TEOS, line width, line height and optical constants of an aSi line, and the diameter and sidewall angle of for the vias. Optical constants of the Si substrate were well characterized and therefore known.

To determine the initial parametric range of the TEOS layer, experimental scatterfield curves were obtained for the blanket layer of TEOS with the same thickness as that of the overlay stack above the aSi lines. This was compared to a simulation library where the TEOS layer thickness was varied from 160 nm to 290 nm and n was varied from 1.32 to 1.622 (k has a value of zero). This process narrowed down the thickness and n ranges to (165 nm to 185 nm) and (1.55 to 1.622) respectively, as shown in Fig.11(f). Repeating a similar procedure for an aSi blank layer, we narrowed down the layer thickness (the aSi line height) range to (90 nm to 100 nm). For the current work we assumed the optical constants for the aSi line to be known as $n = 5.367$ and $k = 0.572$.

Having determined these initial parametric ranges, we then proceeded to do a full parametric fit for the complete overlay stack with a six-parameter fit for multiple overlay values. The parameters that were varied and the best-fit values are: TEOS layer height = 270 nm, TEOS optical constant $n = 1.6$, aSi line width = 130 nm, aSi line height = 100 nm, Via diameter = 160 nm, Via sidewall angle = 85 degrees. Under the constraints used for the simulations the best-fit intensity curves are shown in Fig. 14. This initial parametric fitting run shows promise for the coarse grid simulation values used. Although a finer grid size increases the computation time, the fit and resolution typically improve. This is the next step in this parametric scatterfield overlay study.

5. CONCLUSIONS

We studied the suitability of grating type of targets for overlay measurements. For this type of target that produces only zeroth order specular reflection and imaging for given experimental conditions, there may not be sufficient sensitivity to overlay if there is not adequate optical interaction between the overlay features. This condition should be satisfied in both the vertical and the horizontal directions.

4.1 Experimental evaluation of overlay sensitivity

In this initial attempt to use the scatterfield microscopy for overlay analysis, we first investigated experimental overlay sensitivity for two types of targets. The first type of grating target is a via in TEOS layer over aSi lines. Its cross section is similar to the LVOL target shown in Fig. 5. The experimental sensitivity to the two scan directions and for the two polarizations is shown in Figs. 12(a) to (d) for zero and 25 nm nominal overlay. For this structure, the perpendicular scans with the two polarizations show clear distinction for the two overlay values. Parallel scan direction for both the polarizations shows less sensitivity (Figs. 12(c) and (d)). The second type of target has trenches in a TEOS layer over aSi lines. The experimental overlay sensitivity for zero and 25 nm overlay is shown in Fig. 13. Similar to the via overlay stack, this target stack shows clear sensitivity for the two overlay values when analyzing the perpendicular scan direction data.

In this initial study we experimentally demonstrated suitability of small targets for overlay measurement using two relatively new optical techniques based on a modified bright field optical microscope. Stacking the intensity profiles acquired in an optical microscope as a target is scanned along the focus results in a TSOM image. Using the TSOM imaging method we presented simulated overlay measurements for small in-chip type targets containing either one or three lines (for different stacks). The in-chip type targets are not constrained by sensitivity limitations due to vertical or horizontal optical proximity effects as the dense zeroth order grating targets. Under the simulation conditions studied, the TSOM method for overlay exhibited robust performance to both process variations and optical aberrations.

Placing a small scanning aperture at the conjugate back focal plane of an optical microscope enables collection of scatterometry type angle-resolved reflection curves using a bright field optical microscope. The optical platform that enables this is called scatterfield microscopy. The main advantage of scatterfield microscopy is that the high magnification optical platform allows measurements of very small targets or the simultaneous measurement of an array of targets. The high magnification facilitates usage of small grating type overlay targets on a few microns in size. In the current work, we demonstrated experimental sensitivity to overlay using the scatterfield microscopy technique. We also demonstrated a parametric fitting routine for overlay measurements where we evaluated the optical constants and thicknesses of unknown materials to limit the main overlay simulation library size and obtain improved parametric fits.

5. ACKNOWLEDGEMENTS

The authors acknowledge Thom Germer of NIST for OPTICAL model development. The NIST Office of Microelectronics Programs is gratefully acknowledged for financial support as well as the NIST Scatterfield Competence project. The authors thank Sematech and the NanoFab of NIST for wafer fabrication and measurement support.

6. REFERENCES

1. Richard M. Silver, Bryan M. Barnes, Ravikiran Attota, Jay Jun, Michael Stocker, Egon Marx, and Heather J. Patrick, "Scatterfield microscopy for extending the limits of image-based optical metrology," *Appl. Opt.* 46, 4248-4257 (2007).
2. Heather J. Patrick, Ravikiran Attota, Bryan M. Barnes, Thomas A. Germer, Ronald G. Dixon, Michael T. Stocker, Richard M. Silver, and Michael R. Bishop, "Optical critical dimension measurement of silicon grating targets using back focal plane scatterfield microscopy," *J. Micro/Nanolith. MEMS MOEMS* 7, 013012-1-10, 2008.
3. Richard M. Silver, Bryan M. Barnes, Alen Heckert, Ravikiran Attota, Ronald G. Dixon, Jay Jun, "Angle resolved optical metrology," *Proc. SPIE Int. Soc. Opt. Eng.* 6922, 69221M-1-12, (2008).
4. Ravikiran Attota, Richard M. Silver, and James Potzick, "Optical illumination and critical dimension analysis using the through-focus focus metric," *Proc. SPIE*, 6289, p. 6289Q-1-10 (2006).
5. Ravikiran Attota, Richard M. Silver, and Bryan M. Barnes, "Optical through-focus technique that differentiates small changes in line width, line height, and sidewall angle for CD, overlay, and defect metrology applications," *Proc. SPIE* 6922, 6922OE-1-13, (2008).
6. Ravikiran Attota, Thomas A. Germer, and Richard M. Silver, "Through-focus scanning-optical-microscope imaging method for nanoscale dimensional analysis," *Optics Letters*, Vol. 33, Issue 17, pp. 1990-1992, (2008).
7. Chandra Saravanan, Yongdong Liu, Prasad Dasari, Oleg Kritsun, Catherine Volkman, Alden Acheta, and Bruno La Fontaine, "Evaluating Diffraction Based Overlay Metrology for Double Patterning Technologies", *Proc. SPIE*, 6922, p. 62890C-1-12 (2008).
8. R. Attota, R. M. Silver, M. Bishop, E. Marx, J. Jun, M. Stocker, M. Davidson, and R. Larrabee, "Evaluation of New In-chip and Arrayed Line Overlay Target Designs," *Proc. SPIE*, 5375, p. 395-402 (2004).